Simulation of the hot core mode of arc attachment at a thoriated tungsten cathode by an emitter spot model

2014 Plasma Sources Sci. Technol. 23 054005

(http://iopscience.iop.org/0963-0252/23/5/054005)

IOP Publishing Plasma Sources Science and Technology

Plasma Sources Sci. Technol. **23** (2014) 054005 (13pp) doi:10.1088/0963-0252/23/5/054005

Simulation of the hot core mode of arc attachment at a thoriated tungsten cathode by an emitter spot model

A Bergner[1], F H Scharf[2], G Kühn[3], C Ruhrmann[1], T Hoebing[1], P Awakowicz[1] and J Mentel[1]

[1] Ruhr University Bochum, Electrical Engineering and Plasma Technology, D-44780 Bochum, Germany
[2] Ruhr University Bochum, Theoretical Electrical Engineering, D-44780 Bochum, Germany
[3] Max Planck Institute for Gravitational Physics, Albert Einstein Institute, Callinstrasse 38, 30167 Hannover, Germany

E-mail: bergner@aept.ruhr-uni-bochum.de

Received 17 January 2014 , revised 9 April 2014
Accepted for publication 29 April 2014
Published 25 September 2014

Abstract

Recently, a constricted attachment of an atmospheric pressure low-current argon arc in the centre of the flat end face of a thoriated tungsten cathode was observed and spectroscopically analysed. Its diameter of 0.6 mm and its length of the free standing part of 10 mm are the typical dimensions of electrodes for high-intensity discharge lamps. This paper gives a physical interpretation of the axially symmetric arc spot by a simulation of its properties with a cathodic sheath model which takes into account a reduction in the work function above a critical temperature of the cathode surface by a thorium ion current.

At first the optical observation and spectroscopic investigations are recapitulated. Then, an overview is given on the essential elements which are needed to simulate the cathodic arc attachment on a hot electrode. A simulation of a central cathode spot with these elements gives results which are far away from the experimental findings if a constant work function ϕ is used. Therefore, a temperature-dependent work function $\phi(T)$ is introduced. This $\phi(T)$ transitions from 4.55 to 3 eV above temperatures of the order of 3000 K. With this emitter spot model a constricted arc attachment is obtained by simulation in the centre of the flat end face of the cathode in accordance with experiment. For currents below $i_{\mathrm{arc,max}} \approx 15.5$ A, two spot solutions with different cathode falls are found. They form a current–voltage–characteristic consisting of two branches which extend from a turning point at $i_{\mathrm{arc,max}}$ to lower currents. For $i_{\mathrm{arc}} > i_{\mathrm{arc,max}}$, only a diffuse mode of cathodic arc attachment is obtained. It is shown by a comparison with measured data for $i_{\mathrm{arc}} = 7.5$, 10, 12.5 and 15 A that the solution with the lower cathode fall is observed experimentally.

Keywords: emitter effect, HID lamp, thoriated electrode, arc discharge, emission spectroscopy, simulation

(Some figures may appear in colour only in the online journal)

1. Introduction

An account was given in several papers of a research group at the University of Hannover [1–4] of a special mode of constricted arc attachment on a thoriated tungsten cathode. Electrodes of this kind are used in high-intensity discharge (HID) lamps. The constricted attachment of the atmospheric pressure argon arc was quite different from the diffuse mode of arc attachment also being observed at the same cathode and under identical operating conditions. The original authors called it 'blue core' mode by reason of its special appearance. The arc plasma within the constriction zone in front of the cathode was investigated by careful spectroscopic measurements of the spatially resolved electron temperature $T_{\mathrm{e}}(\vec{r})$, electron density $n_{\mathrm{e}}(\vec{r})$ and gas temperature $T_{\mathrm{g}}(\vec{r})$ [2–4]. Peak values of the order of $T_{\mathrm{e}} = 21\,000$ K, $n_{\mathrm{e}} = 2 \times 10^{23}$ m^{-3}, and a gas temperature of the order of $T_{\mathrm{g}} = 12\,000$ K were measured within the constriction zone. They are much higher

than within the plasma boundary layer in front of the cathode formed by a diffuse mode of arc attachment [3]. Therefore, the authors later called the constricted arc attachment 'hot core' mode.

The 'hot core' mode differs from other constricted cathodic arc attachments shown in [5–9] by its rotational symmetry with respect to the axis of the electrode. The difference is confirmed by the failed attempts to simulate the special constricted arc attachment on the cathode in accordance with the experimental results in a similar manner as in [10] or in [11] with a cathodic boundary layer model given in [12] or a similar one given in [13]. However, its shape is very similar to the so-called emitter spot, which is observed in high-pressure metal halide (MH) lamps. It was initially observed on a tungsten cathode, which was operated with a dc current within a lamp tube made of transparent yttrium aluminum garnet (YAG). The discharge was run in a mercury atmosphere, being seeded among other ingredients (NaI, TlI) with DyI_3 [14]. The finding was confirmed by an investigation of the electrode behaviour within the same type of lamps when they were operated with switched dc currents of different amplitudes and operation frequencies [15, 16]. It was also confirmed when the same type of lamps was seeded with TmI_3 [17], CeI_3 or LaI_3 [18, 19].

The emitter spot may be traced back to the so-called gas phase emitter effect induced by a monolayer of atoms on the electrode surface, which reduces the work function of the tungsten electrode. The reduction in the work function is produced by a dipole layer, which can be formed by a large variety of elements being electropositive with reference to tungsten. The gas phase emitter effect of dysprosium, cerium, caesium, thulium, lanthanum and holmium was investigated in a YAG lamp operated with switched dc currents of different operating frequencies by phase-resolved pyrometric measurements of the electrode temperature and phase-resolved spectroscopic measurements of the atom and ion density of the emitter material. The lamps were filled with a mercury atmosphere of 1.3 or 2 MPa, which was optionally seeded with DyI_3 [15, 20–22], CeI_3 or CsI [18, 23], TmI_3 [17, 18, 24], LaI_3 [18] and HoI_3 [25]. It was found that a reduction in the electrode temperature within the cathodic phase is always correlated with an increase in the ion density and, with some time delay, also in the atom density of the emitter material in front of the cathode. Within the anodic phase the opposite was observed, a reduction in the ion and atom density of the emitter material and a missing lowering of the electrode temperature. However, with increasing operating frequency an overlap of the increase in the emitter material density and a reduction in the electrode temperature from the cathodic phase onto the anodic phase was established resulting from a finite lifetime of the atomic monolayer. The findings were interpreted to be caused by an ion current of emitter material onto the electrode within the cathodic phase. This current counteracts with the evaporation of the atomic layer of emitter material from the electrode surface and it may be more important than the adsorption of atomic emitter material, which was originally considered to compensate the evaporation. A rare example for a balance between evaporation and adsorption is given in [26], which shows the reduction in the work function of a tungsten anode in a high pressure sodium discharge lamp operated with a dc current.

The emitter spot in MH lamps may be attributed to a locally enhanced ion current density of emitter material, by which the work function is reduced within a spot on the cathode surface. The ion current density of the emitter material increases together with the total ion current density in dependence on the plasma temperature within the cathodic boundary layer up to a saturation value which is achieved when the plasma is fully ionized. The plasma temperature maximum coincides in general with the centre of the discharge, which may agree at least approximately with the axis of the cathode rod. The reduced work function causes an enhanced thermionic electron emission in the centre of the arc attachment zone, but simultaneously the cathode fall U_c remains nearly constant within the whole plasma boundary layer. It brings about a local increase in the power input into the plasma boundary layer and as a consequence a local increase in the plasma electron temperature and ion current density. The localized reduction in ϕ may be able to initiate a constriction of the arc attachment onto the centre of the cathode end face.

Results of pyrometric temperature measurements for pure and thoriated tungsten electrodes are compared in [27]. The measurements were performed in the Bochum model lamp [28], in which atmospheric pressure argon arcs were operated with dc currents of different amplitudes. A diffuse mode of arc attachment was realized on cathodes with the same dimensions as in [3, 4]. Doping the electrode with ThO_2 caused a reduction in the cathode temperature of the order of 1000 K. Moreover, it was noted that the reduction is independent of the amount of ThO_2, by which the electrode material is doped. The temperature reduction corresponds to a lowering of the work function ϕ of the cathode from 4.55 to 3 eV as was shown by a comparison with cathode temperatures obtained by a numerical simulation of the diffuse mode of arc attachment with a well-established boundary layer model [10, 12]. On the other hand the anode temperature is not reduced but weakly increased by a doping with ThO_2. The weak influence of ThO_2 on the anode temperature confirms the previous finding [29, 30] that the average work function of the anode does not depend on the thorium content of the electrode. The results can be explained by a thorium ion current, by which evaporated thorium is repatriated to the hot cathode surface, but not to the anode.

This paper aims to an interpretation of the 'hot core' mode. The conditions in front of the thoriated electrode are quite similar to those in front of a cathode in a MH lamp seeded with emitter material. This is especially the case if the thorium content within the electrode tip is depleted after a longer running time of the electrode but thorium is still evaporated from the lateral area of the electrode and carried by convection into the discharge. Within the discharge it is ionized and transported by cataphoresis to the cathode. The 'hot core' mode may be interpreted as an emitter spot, if this supply of the cathode tip with thorium applies. This possibility is investigated subsequently by a simulation according to [10] with a modified version of the cathodic boundary layer model given in [12]. It is accomplished by a temperature-dependent

work function which has a strong influence on the thermionic electron emission determined by the Richardson Dushman equation. A work function of $\phi = 4.55\,\mathrm{eV}$ is applied at low electrode temperatures. It is lowered by a steep decrease in a work function of the order of 3 eV at a transition temperature of the order of $T_{\mathrm{th}} = 3000\,\mathrm{K}$ within a temperature interval of the order of $\tau \approx 20\,\mathrm{K}$.

The spectroscopic investigations of the 'hot core' mode performed in Hannover are recapitulated in the next section. The simulation procedure for hot arc cathodes is described in section 3. The procedure is applied first to simulate a central cathode spot of an argon arc at atmospheric pressure for a tungsten electrode with the same dimensions as those at which the 'hot core' mode is observed. The results are far different from the experimental findings. Subsequently, the emitter spot model is presented and simulation results are presented in dependence on different model parameters T_{th} and τ. Finally, they are discussed by comparing measured and simulated data. The paper is to a large extent an excerpt of Bergner's diploma thesis. The photos and the results of spectroscopic measurements are taken from Kühn's PhD thesis [31]. The results for $i_{\mathrm{arc}} = 7.5, 10.0$ and $15.0\,\mathrm{A}$ are not published in journals up to now, only the results for $i_{\mathrm{arc}} = 12.5\,\mathrm{A}$ are already published in [4]. The full set of data improves the verification of the simulation results.

2. Experimental investigations and results

The hot core mode was observed when a low-current arc was operated in an atmospheric pressure noble gas atmosphere, e.g. argon, between a rod shaped thoriated tungsten cathode and an equally shaped but thicker tungsten anode. They are arranged along a common vertical axis where the anode is positioned at a distance of approximately 10 mm above the cathode. The electrodes are fixed by water cooled holders on the bottom and the top cover of a spacious, vacuum tight aluminum vessel with view ports including windows made of quartz for optical observation. The discharge assumes the shape of a free burning arc within the vessel. An overview of the experimental setup is given in [3], figure 3, or in [4], figure 3.

The vessel at which the spectroscopic measurements are made is formed from a cubic aluminum block with an edge length of 80 mm [4]. The block is caved by three perpendicular drill holes with a diameter of 40 mm along axes positioned in the centre and directed perpendicular to the faces of the cube. The upper part of the cube is closed with a water cooled copper plate. It is the base of an anode holder formed by a cylindrical copper bar which extends from the centre of the plate into the vessel. The anode rod made of pure tungsten with a diameter of 2 mm and a length of 30 mm is inserted into a drilling hole along the axis of the bar. The lower port is closed with a similar water cooled copper plate in the centre of which a cylindrical copper bar arises with a central drilling hole to hold the cathode rod with a diameter of 0.6 mm and a length of 30 mm. The length of the free-standing part of both electrodes amounts to $l_{\mathrm{E}} = 10\,\mathrm{mm}$. Both copper plates are separated from the aluminum block by an insulating plate made of polyoxymethylene (POM). One side port is connected to the vacuum pump system and the opposite one is used for monitoring the discharge with a standard video CCD camera. The two other side ports are also equipped with optical windows. One of these was used for coupling in a pulsed Nd : YAG laser to accomplish an easy, reproducible and clean ignition of the discharge. After ignition the discharge vessel was moved to a different beam path by a stepper motor, and the port was used for optical monitoring of the electrodes and of the arc between them. The remaining port was used to carry out spectroscopic measurements that are described below. Figure 1 shows four pictures of the 'hot core' mode of cathodic arc attachment taken at the current amplitudes $i_{\mathrm{arc}} = 7.5, 10.0, 12.5, 15.0\,\mathrm{A}$. The cathode having the dimensions $r_{\mathrm{E}} = 300\,\mu\mathrm{m}$, $l_{\mathrm{E}} = 10\,\mathrm{mm}$ was doped with 1.8% ThO_2 of the total electrode volume (G18 material).

A lateral view of the plasma in front of the cathode, shown in figure 1, is imaged with a special optical system onto the entrance slit of a grating spectrograph. The spectrograph has two optional exit ports. The image plane of one port is equipped with a slow scan CCD camera for measurements at a stationary discharge and the image plane of the other port with an ICCD camera for measurements with high temporal resolution. The axis of the vertically burning arc is imaged perpendicular to the entrance slit of the spectrograph, using a so-called mirror tower. The slit records the light emission of an arc cross section in an adjustable distance z from the electrode tip. The two-dimensional image on the CCD camera sensor represents the surface radiance $I_\lambda(x, z)\,\mathrm{d}\lambda = I_\nu(x, z)\,\mathrm{d}\nu$ as a function of the distance x from the arc axis along the slit and in dependence on λ or ν perpendicular to the slit. The counts of the CCD pixels were calibrated with a tungsten ribbon lamp in units of $\mathrm{W\,m^{-2}\,sr^{-1}}$. The radiance $I_\lambda(x, z)$ is related by the Abel transformation to the local spectral volume emission coefficient $\epsilon_\lambda(r, z)$ if the plasma is rotational symmetric and optical thin. Line emission coefficients ϵ_{l} are obtained by a numerical integration over their line profiles. This can be done prior to the inverse Abel transformation by which the emission coefficients are calculated. The spatial resolution in the direction of the axis is determined mainly by the width of the entrance slit of the spectrograph. As a compromise between an appropriate spatial and spectral resolution on the one hand and a reasonable signal-to-noise ratio (SNR) on the other a slit width of $50\,\mu\mathrm{m}$ was chosen. Measurements were carried out at an argon arc at seven different distances ($50, 100, 150, 200, 250, 500, 750\,\mu\mathrm{m}$) from the electrode.

Detailed spectroscopic investigations had shown that a model of partial local thermodynamic equilibrium (pLTE) has to be applied for an appropriate description of the plasma state within the hot core. It is defined by three parameters: the electron temperature T_{e}, the heavy particle temperature $T_{\mathrm{h}} < T_{\mathrm{e}}$ and an underpopulation factor $b < 1$ of all excited states in relation to the atomic ground state of argon. The kinetic energy of the free electrons (Maxwell distribution) and the ratios of the population densities of all excited electronic states (Boltzmann distribution and Saha equilibrium) are specified by T_{e} and the ratio between the density of an excited arbitrary electronic state and the atomic ground state additionally by b. The kinetic energy and the number density of the heavy particles $n_{\mathrm{a}} + n_{\mathrm{i}}$ are given by T_{h}.

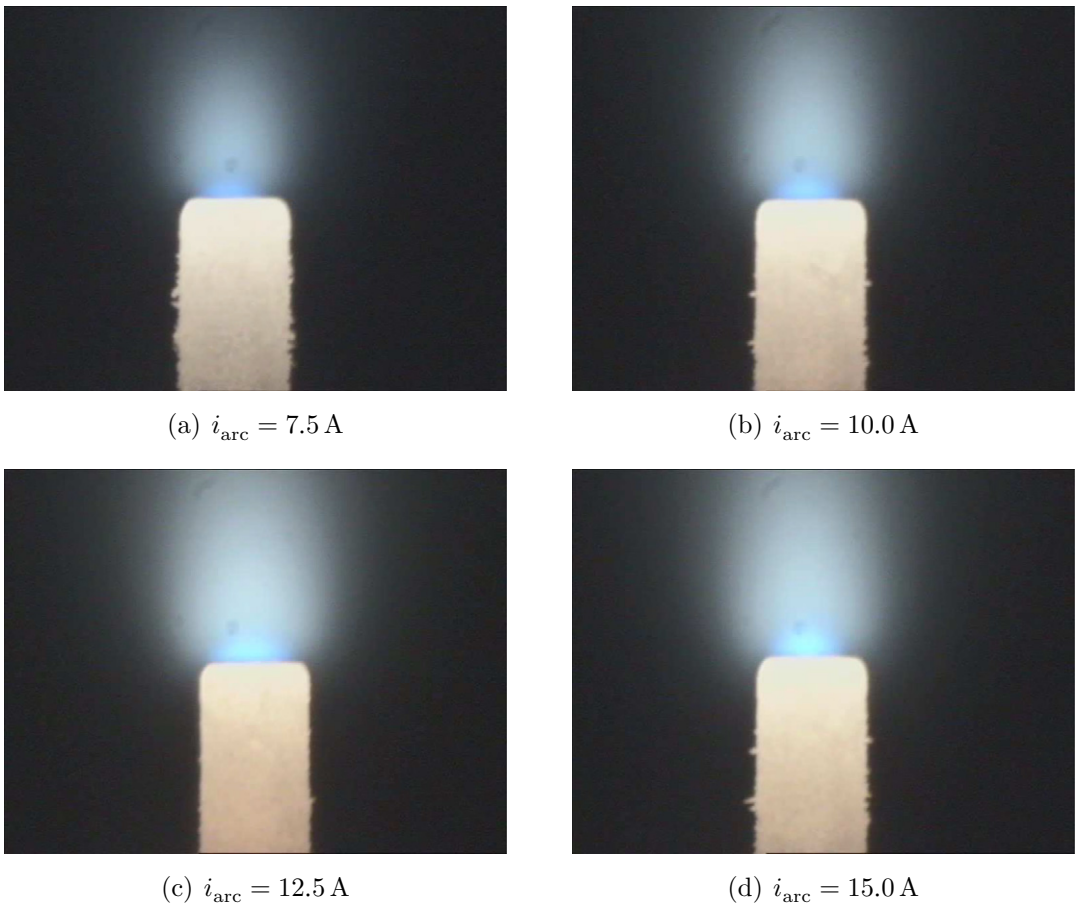

(a) $i_{\mathrm{arc}} = 7.5\,\mathrm{A}$ (b) $i_{\mathrm{arc}} = 10.0\,\mathrm{A}$

(c) $i_{\mathrm{arc}} = 12.5\,\mathrm{A}$ (d) $i_{\mathrm{arc}} = 15.0\,\mathrm{A}$

Figure 1. Pictures of the hot core mode of cathodic arc attachment on a thoriated tungsten electrode with the dimensions $r_{\mathrm{E}} = 300\,\mu\mathrm{m}$, $l_{\mathrm{E}} = 10\,\mathrm{mm}$. (*a*) upper left picture: $i_{\mathrm{arc}} = 7.5\,\mathrm{A}$, (*b*) upper right picture: $i_{\mathrm{arc}} = 10.0\,\mathrm{A}$, (*c*) lower left picture: $i_{\mathrm{arc}} = 12.5\,\mathrm{A}$, (*d*) lower right picture: $i_{\mathrm{arc}} = 15.0\,\mathrm{A}$.

The measurement of three different physical quantities is needed to determine T_{e}, T_{h} and b. Population densities of excited Ar II states were deduced from measured line emission coefficients of argon ion lines emitted within a spectral band between 440 and 443.4 nm. T_{e} (r, z) and the local electron density n_{e} (r, z) were obtained by a combination of the population density of one or a sum of several excited Ar II states with a measurement of the continuum emission coefficient within an interval from 445.5 to 445.6 nm. The required measurements were made with the slow scan CCD camera.

T_{h} was determined by switching off the arc current with a special power interruption technique for a short time, e.g. 20 μs: the interruption is accompanied by a momentary increase in the intensity of Ar I lines. It results from a decay time of the electron temperature T_{e} of the order of one microseconds, in which it falls off to the temperature T_{h} of the heavy particles, and a much longer decay time of the electron density n_{e} of the order of 100 μs. The population densities of the excited Ar I states are strongly coupled by inelastic electron collisions to the electron density n_{e} so that the different time constants cause a transient increase in the population densities of the excited atomic states in relation to n_{e}. The rise in the emission coefficient of the 714.7 nm Ar I line ϵ_{715} to a maximum value $\epsilon_{715}^{\mathrm{max}}$ within approximately 2 μs and the subsequent much slower decrease was determined with a temporal resolution of 200 ns by an analysis of measurements with the ICCD camera. The ratio $T_{\mathrm{e}}/T_{\mathrm{h}}$ was deduced from the relative enhancement of $\epsilon_{715}^{\mathrm{max}}$ with respect to the stationary value of ϵ_{715}.

Figure 2(*a*) shows radial distributions of the electron temperature $T_{\mathrm{e}}(r)$ and the heavy particle temperature $T_{\mathrm{h}}(r)$ measured at a distance $z = 50\,\mu\mathrm{m}$ from the electrode surface, figure 2(*b*) axial distributions $T_{\mathrm{e}}(z)$ and $T_{\mathrm{h}}(z)$ on the arc axis ($r = 0$), both at current amplitudes $i_{\mathrm{arc}} = 7.5, 10.0, 12.5, 15.0\,\mathrm{A}$. The simulation delivers only electron and heavy particle temperatures within the cathodic boundary layer of some micrometre thickness. To compare them with measurements in figure 2(*b*) the attempt is made to extrapolate $T_{\mathrm{e}}(r = 0, z)$ and $T_{\mathrm{h}}(r = 0, z)$ to $z = 0$. Since the power input into the cathodic boundary layer is distinctly higher than within the bulk plasma and with it the electron temperature the extrapolation of $T_{\mathrm{e}}(r = 0, z)$ to higher values for $z = 0$ may deliver at least a lower limit for $T_{\mathrm{e}}(r = 0, z = 0)$, which is not far away from the real electron temperature. But the extrapolation of $T_{\mathrm{h}}(r = 0, z)$ to lower values for $z = 0$ may deliver very high temperatures $T_{\mathrm{h}}(r = 0, z = 0)$ since its steep decrease to the electrode surface temperature takes mainly place within the cathodic boundary layer.

The courses of $T_{\mathrm{e}}(r)$ and $T_{\mathrm{h}}(r)$ reflect the hot core mode of arc attachment by a lift of $\Delta T_{\mathrm{e}} \approx 5000\,\mathrm{K}$ from the edge of

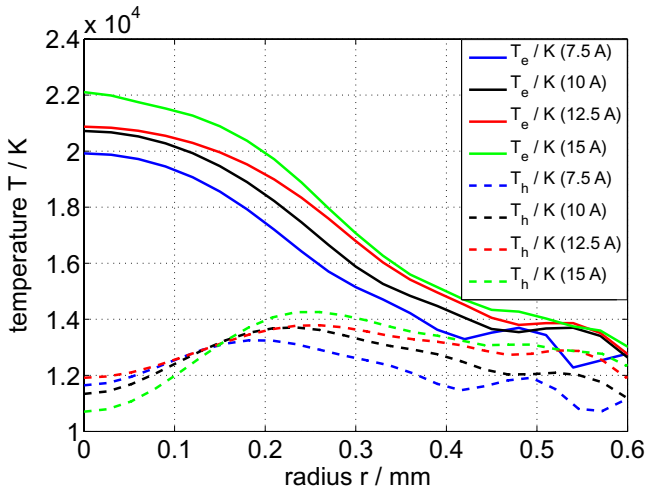

(a) $T_e(r), T_h(r)$

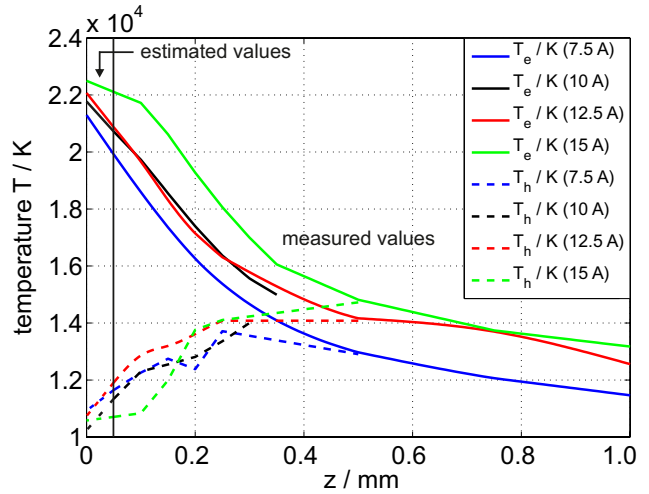

(b) $T_e(z), T_h(z)$

Figure 2. Temperature distributions measured in front of the end face of a thoriated tungsten cathode at current amplitudes $i_{arc} = 7.5, 10, 12.5, 15$ A. The electrode dimensions are $r_E = 300\,\mu$m, $l_E = 10$ mm. (*a*) Radial distributions T_e (r) and T_h (r) at a distance of 50 μm. (*b*) Temperature distributions $T_e(z)$ and $T_h(z)$ along the arc axis ($r = 0$).

the end face and from the arc column to its centre. A doubling of the arc current from 7.5 to 15 A produces an increase in $T_e(r = 0)$ of about 10% from 20 000 to 22 000 K. The courses of $T_h(r)$ show a smooth increase from a flat minimum on the arc axis towards a flat maximum at the edge of the blue core of the discharge at $r \geqslant 200\,\mu$m, and a subsequent weak decrease. The temperature minima indicate a strong cooling of that part of the plasma in front of the cathode which is characterized by the emission of blue argon ion lines. A discussion of the power balance of the heavy particles within the cathodic boundary layer in the next section will confirm that it is mainly cooled by emitting an ion current to the cathode. The low value of $T_h(r = 0, z = 50\,\mu\text{m})$ for $i_{arc} = 15$ A may be no measuring error but the effect of an enhanced ion current density. The cooling of the heavy particles in front of the cathode is confirmed by the decline of $T_h(r)$ with decreasing distance z.

The large difference $T_e - T_h$ in front of the cathode reflects the high electrical power input per unit volume $j^2\sigma^{-1}$ into the plasma where j denotes the current density and σ the electrical conductivity of the plasma

$$\sigma = \frac{e^2 n_e}{m_e \nu_e}. \tag{1}$$

The electrical power is absorbed by the electrons and predominantly transferred by elastic collisions to the heavy particles. If this assumption is valid the local power balance of the electrons reads [32]

$$\frac{j^2}{\sigma} = \frac{3m_e}{M_{Ar}} k_B (T_e - T_h) \nu_e n_e. \tag{2}$$

Inserting σ, the electron power balance can be used to express the current density j by the electron density n_e and the temperature difference $T_e - T_h$:

$$j = \sqrt{3} e n_e \sqrt{\frac{k_B (T_e - T_h)}{M_{Ar}}}, \tag{3}$$

ν_e is the collision frequency of the electrons with atoms and ions and M_{Ar} is the mass of argon atoms. All other quantities have the usual meaning.

Values of n_e measured at a distance $z = 50\,\mu$m from the electrode surface are given in figure 3(*a*). Values of $T_e - T_h$ can be taken from figure 2(*a*). Inserting both quantities into equation (3) delivers $j(r)$ at $z = 50\,\mu$m for $i_{arc} = 7.5, 10, 12.5, 15$ A. The resulting courses $j(r)$ are shown in figure 3(*b*) for comparison with $j(r)$-distributions within the cathodic boundary layer obtained by simulation.

3. Simulation of hot arc cathodes

An approved method to simulate hot arc cathodes is based on the concept of transfer functions [33]. It acts on the assumption that the power flux density q_p and the current density j supplied by the cathodic boundary layer to the cathode surface are only dependent on the local surface temperature T_c and the cathode fall U_c:

$$q_p = q_p(T_c, U_c) \tag{4}$$

$$j = j(T_c, U_c). \tag{5}$$

U_c is taken constant within the layer. The concept reflects the fact that the cathodic boundary layer is microscopically thin but the density of power fed into the layer and the gradients at its borders are so high that only the electrons which are emitted thermionically from the cathode surface act upon the boundary layer from outside. The influence of the arc plasma on the boundary layer can be neglected. The power flux density q_p is related to the local power balance of the boundary layer according to

$$q_p(U_c, T_e) = \left(U_c - \phi - \left(\frac{5}{2} + 0.7\xi \right) \frac{k_B T_e}{e} \right) j. \tag{6}$$

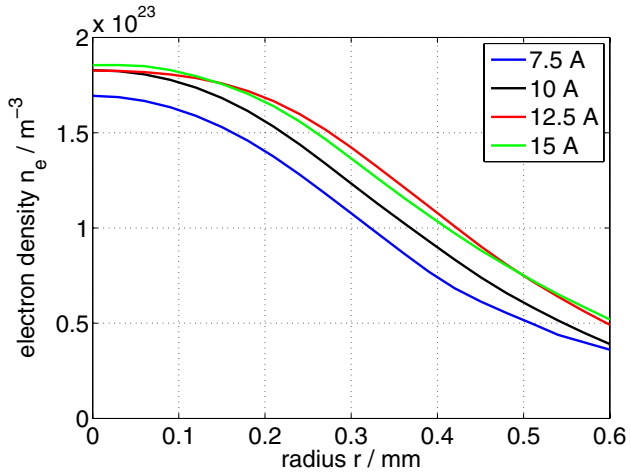

(a) $n_e(r)$

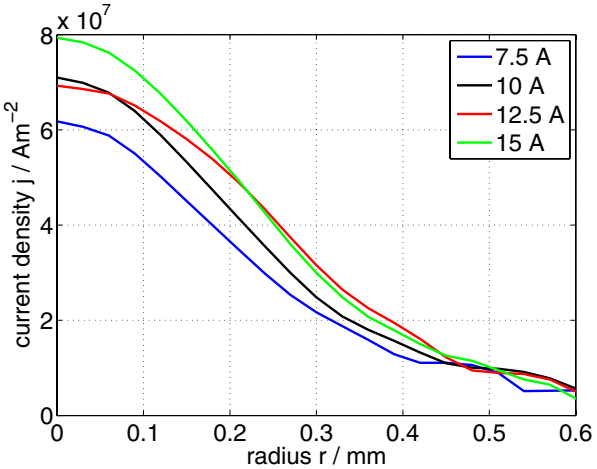

(b) $j(r)$

Figure 3. Radial electron density distribution and current density distributions at a distance of 50 μm from the end face of a tungsten cathode at current amplitudes $i_{arc} = 7.5, 10, 12.5, 15$ A. The electrode dimensions are $r_E = 300\,\mu$m, $l_E = 10$ mm. (*a*) Measured electron density distribution $n_e(r)$. (*b*) Calculated current density distribution $j(r)$.

The current density j at the surface is composed of different partial current densities:

$$j = j_{em}(T_c) + j_i(T_e) - j_{ep}(T_e), \tag{7}$$

$j_{em}(T_c)$ is the density of the electron current emitted thermionically by the cathode surface, $j_i(T_e)$ is the ion current density supplied by the cathodic boundary layer and $j_{ep}(T_e)$ is the density of the electron back diffusion current from the plasma boundary layer to the cathode. T_e is the local electron temperature within the plasma boundary layer. The terms in the bracket on the right-hand side of equation (6) represent the cathode fall U_c, the work function ϕ and the electron enthalpy flux from the cathodic boundary layer to the arc plasma $(\frac{5}{2} + 0.7\xi)\frac{k_B T_e}{e}$, given in volts. The difference $U_c - \phi$ is considered to be constant along the whole cathode boundary layer, since the reduction in the work function $\Delta\phi$ by the Schottky effect is compensated by the same reduction in the cathode fall. $0.7\xi\frac{k_B T_e}{e}$ is a correction term, which has to be taken into account if the ionization degree ξ on the plasma side of the boundary layer approaches $\xi = 1$. Equation (6) was discussed in detail in [12] (see equations (2)–(4) in [12]).

The transfer functions are calculated with a special cathodic boundary layer model. It is composed of a sheath which takes into account deviation from quasi-neutrality but neglects collisions and of a pre-sheath which takes into account collisions (charge transfer and ionization collisions) but assumes quasi-neutrality [12]. It is terminated on the plasma side by the so-called Saha plasma. The charged particle density in it is determined by the Saha equation in dependence on T_e and by Dalton's law, in which in addition the temperature of the heavy particles $T_h < T_e$ is considered. An underpopulation factor b, which was found experimentally, is not taken into account. A small additive of thorium vapour within the argon plasma may have only a weak influence on its transfer functions [34, 35]. It is not taken into account. The voltage drop along the sheath is U_s and along the pre-sheath $U_p = U_c - U_s$. The ions generated within the pre-sheath are accelerated by the voltage drop U_p to a velocity at the sheath edge which exceeds the ion sound velocity. According to the Bohm criterion the ion sound velocity is required for the formation of a stable space charge layer.

Power balances of the electrons and of the heavy particles within the layer are used to determine an average electron temperature T_e and an average heavy particle temperature T_h within the layer as a function of T_c and U_c. T_h coincides with the gas temperature T_g for conditions considered in this paper. The power balance of the electrons given in [12, 27] is rather voluminous, a simplified version being formed by the two dominant terms, reads as

$$j_{em}(T_c, \phi)U_c \approx j_i(T_e)U_i. \tag{8}$$

The left-hand side represents the power being transferred by the cathode fall U_c to the electrons, which are emitted by the cathode surface. It is mainly consumed to produce an ion current towards the cathode by impact ionization. The power consumption is given by the right-hand side of equation (8), where eU_i is the ionization energy of the filling gas. It demonstrates clearly the existence of a definite relation between T_e and T_c.

It is sufficient to consider only the pre-sheath in more detail for setting up the power balance of the heavy particles since collisions are neglected within the sheath. It reads

$$\eta j_i U_p + j_i \frac{2k_B T_c}{e} = j_i \left(0.875\frac{k_e T_c}{e} + 1.65\frac{k_B T_h}{e}\right) + \alpha\,(T_h - T_c)\,. \tag{9}$$

The first term on the left-hand side represents the electrical power supplied to the ions by the voltage drop U_p at the pre-sheath. The factor $\eta < 1$ takes into account that the ion current density increases within the pre-sheath from zero at the side of the bulk plasma to the maximum value j_i at the sheath edge. The calculation of η can be found in [12] or [27]. The particle flux density of neutrals is j_i/e produced by the neutralization of ions at the cathode and $2k_B T_c$ the average enthalpy withdrawn by the neutrals from the cathode. The first term on the right-hand side represents the flux density of kinetic energy

transferred from the pre-sheath to the sheath. The second term on the right-hand side of equation (9) considers the heat transfer from the heavy particles in the boundary layer to the cathode. It is represented by the temperature difference $T_h - T_c$ and an empirical heat transfer coefficient α. An appropriate value is $\alpha = 5000\,\mathrm{Wm^{-2}K^{-1}}$ as was shown in [36]. The term $j_i U_s$ has to be added on both sides of equation (9) to complete the power balance of the heavy particles within the cathodic boundary layer (see equations (44) and (45) of [12] for a more detailed discussion).

A computer program on the basis of this model is used to calculate $q_p(T_c, U_c)$ and $j(T_c, U_c)$ for specified values of T_c and U_c.

The differential heat conduction equation

$$\nabla \cdot (\kappa \nabla T) = 0 \tag{10}$$

has to be integrated to determine the shape of the arc attachment on the cathode tip. The integration has to be performed for a rod shaped rotationally symmetric tungsten electrode. Its dimensions are given by a radius r_E, length l_E and the edge radius of the end face of the electrode r_{edge}. A sketch of the solution area is given in figure 4. Values for the temperature-dependent heat conductivity $\kappa(T)$ are taken from [37]. Boundary conditions are required e.g. on the electrode surface to integrate the second order partial differential equation. A constant temperature T_F is assumed within the cross section of the electrode rod which is coplanar with the end face of the electrode holder.

$$T(z = 0) = T_F = \text{const.} \tag{11}$$

At the free surface of the electrode a heat flux takes place, which is determined by the local surface temperature T_c. It is composed of the power flux from the plasma to the cathode represented, according to equation (6), by $q_p(T_c, U_c)$ and the thermal radiation emitted by the electrode surface:

$$q_{rad}(T_c) = \sigma_{SB} \epsilon_{tot}(T_c)(T_c^4 - T_{amb}^4) \tag{12}$$

σ_{SB} is the Stefan–Boltzmann constant, $\epsilon_{tot}(T_c)$ is the total emissivity of tungsten in dependence on the surface temperature T_c [38] and T_{amb} the ambient temperature of the electrode. Its choice, $T_{amb} = 300\,\mathrm{K}$, is not very critical. Applying the surface perpendicular unit vector $\vec{n}$ the boundary condition at the free electrode surface reads:

$$\vec{n} \cdot \kappa(T_c)(\nabla T)_{T=T_c} = q_p(T_c) - q_{rad}(T_c). \tag{13}$$

The arc current i_{arc} transferred to the cathode is related to the cathode fall U_c by the surface integral of the current density $j(T_c, U_c)$ over the cathode surface:

$$i_{arc}(U_c) = \int_A j(T_c, U_c)\vec{n} \cdot \mathrm{d}\vec{A}. \tag{14}$$

The inverse function $i_{arc}(U_c)$ is calculated with equation (14) for a set of cathode falls U_c to obtain the current–voltage-characteristic (CVC) $U_c(i_{arc})$.

A commercial finite element (FEM) solver is used to generate numerical solutions of the heat conduction equation.

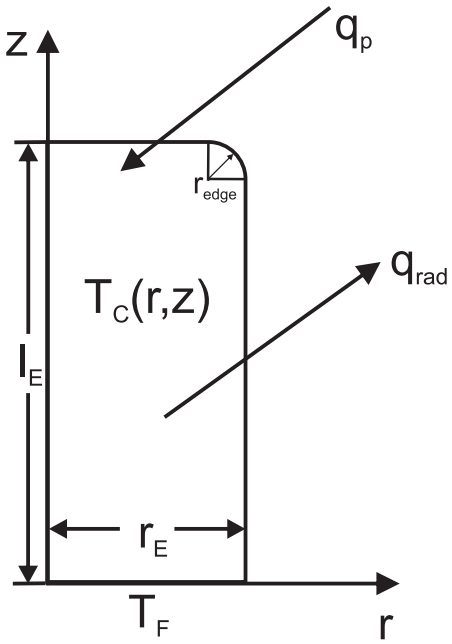

Figure 4. Sketch of the solution area for the numerical simulation.

It is a pre-defined problem within the program. Therefore, it is only necessary to define physical constants, material coefficients, boundary conditions and a solution area, which can be of arbitrary geometry. On this area a computational grid consisting of finite elements has to be specified. Since the shape of the hot core is rotationally symmetric, a two-dimensional solution area with the same symmetry is chosen. The simulation is done iteratively. A temperature distribution $T(\vec{r})$ has to be specified as an initial condition within the solution area. In the case of the diffuse mode it is sufficient to preset a linearly increasing temperature distribution along the axis of the electrode and a constant temperature within the electrode cross sections. An inhomogeneous temperature increase has to be added on the electrode surface to simulate a constricted arc attachment. It was found out that a $\cos(\frac{\pi}{2}\frac{r^2}{R^2})$-distribution at the electrode end face is an efficient starting point to simulate a constricted rotational symmetric arc attachment. The program starts with these initial conditions and converges regularly after a few iteration steps. To get $U_c(i_{arc})$ the simulation is repeated for a certain set of cathode falls U_c.

4. Simulation of a central cathode spot

Attempts were made to simulate a cathode spot mode of arc attachment on a flat thoriated tungsten electrode as used in [4]. The corresponding solutions were numerically unstable as predicted by [39, 40]. To overcome the problem, a dome-shaped electrode tip was chosen. Simulations of a central cathode spot were performed on the sphere hat of a tungsten electrode with a work function of $\phi = 3\,\mathrm{eV}$ and $\phi = 4.55\,\mathrm{eV}$. The resulting CVCs $U_c(i_{arc})$ of the central cathode spot and for comparison also of the diffuse mode of arc attachment are given in figures 5(*a*) and 5(*b*). The CVCs of the central spot consist—as in many other cases [10, 11]—of two branches

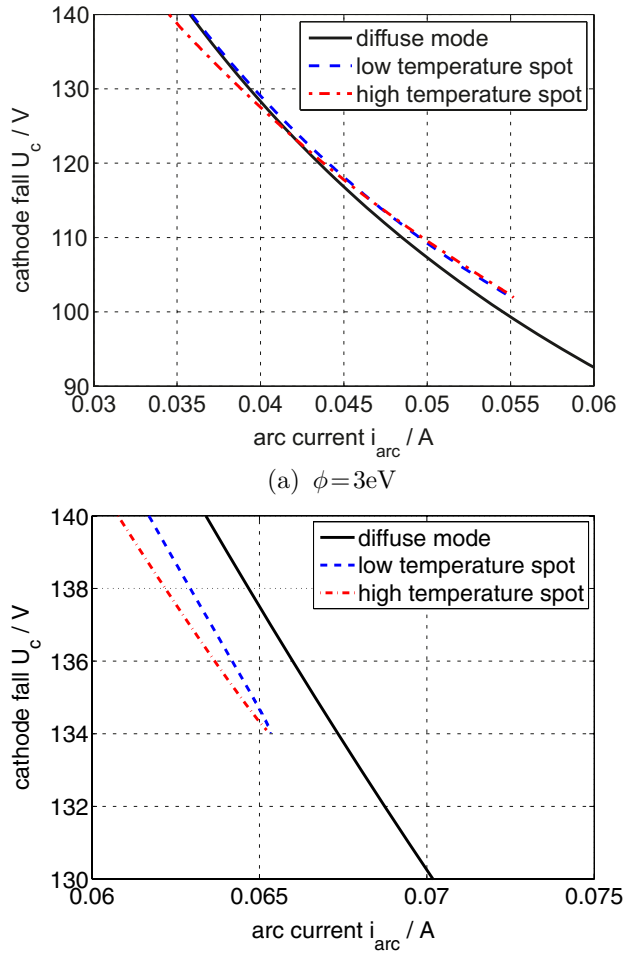

Figure 5. Current–voltage characteristic $U_c(i_{arc})$ of the cathodic boundary layer of a central spot formed by an atmospheric pressure argon arc on the spherical end face of a thoriated tungsten cathode for $\phi = 3\,\mathrm{eV}$ (*a*) and $\phi = 4.55\,\mathrm{eV}$ (*b*). Its dimensions are $r_E = 300\,\mu\mathrm{m}$, $l_E = 10\,\mathrm{mm}$. In addition, $U_c(i_{arc})$ of the diffuse mode is shown. The CVCs are obtained by simulation.

which differ for a fixed current i_{arc} by U_c and by the maximum value of the cathode temperature T_c on the electrode tip. They are linked in a reversal point at the highest current at which the central spot is able to exist in addition to the diffuse mode. The CVCs do not differ very much from the characteristics of edge spots at cathodes with the same dimension but with a flat end face. Figure 5 shows that the current i_{arc} at which the central spot is viable is more than two orders of magnitude lower than i_{arc}, at which the hot core mode is observed both at $\phi = 3\,\mathrm{eV}$ and $\phi = 4.55\,\mathrm{eV}$ as is shown by the examples in figure 1. The cathode spots given in figure 5 correspond rather to the cathodic roots of a spark discharge. This means that the attempt of an interpretation of the hot core mode by a central cathode spot has failed if realistic but constant values of ϕ are assumed.

5. Emitter spot model

In a next step a temperature-dependent work function ϕ is introduced to accomplish a simulation of the hot core mode in accordance with the experimental findings. At a low surface temperature T_c a high work function ϕ_1 and at a high electrode temperature a low work function ϕ_2 is assumed. It takes into account a thorium ion current by which a thorium mono-layer spot is sustained within a patch on the hot tungsten surface. The variation of the work function in dependence on the surface temperature T_c is modelled by a weight function $w_1(T_c)$ for ϕ_1 and a weight function $w_2(T_c)$ for ϕ_2:

$$\phi(T_c) = w_1(T_c)\phi_1 + w_2(T_c)\phi_2. \tag{15}$$

The weight functions $w_1(T_c)$ and $w_2(T_c)$ are defined by

$$w_1(T_c) = \frac{1}{1 + e^{\frac{T_c - T_{th}}{\tau}}} \tag{16}$$

$$w_2(T_c) = 1 - \frac{1}{1 + e^{\frac{T_c - T_{th}}{\tau}}} = 1 - w_1(T_c). \tag{17}$$

Accordingly their sum is normalized to 1. The courses of $w_1(T_c)$ and $w_2(T_c)$ are determined by the parameters T_{th} and τ. T_{th} specifies the transition temperature, at which the work function ϕ changes from ϕ_1 to ϕ_2 and τ the width of the temperature interval, within which the transition takes place.

Only some minor changes are needed within the computer program by which $q_p(T_c, U_c)$ and $j(T_c, U_c)$ can be calculated to take into account the temperature-dependent work function $\phi(T_c)$ being given by equation (15). In figure 6 an example for $q_p(T_c)$ is given for $U_c = 10\,\mathrm{V}$, $\phi_1 = 4.55\,\mathrm{eV}$, $\phi_2 = 3\,\mathrm{eV}$, $T_{th} = 3000\,\mathrm{K}$ and $\tau = 20\,\mathrm{K}$. The value $\phi_1 = 4.55\,\mathrm{eV}$ represents the average work function of pure tungsten, and $\phi_2 = 3\,\mathrm{eV}$ the minimum work function of thoriated tungsten. It may be the result of a self-adjustment as in the case of a thoriated cathode being operated in the diffuse mode [27]. The resulting power flux density is supplemented by the courses of $q_p(T_c, U_c = 10\,\mathrm{V})$ for the constant work functions $\phi_1 = 4.55\,\mathrm{eV}$ and $\phi_2 = 3\,\mathrm{eV}$. The reduction in the work function from $\phi_1 = 4.55\,\mathrm{eV}$ to $\phi_2 = 3\,\mathrm{eV}$ causes a displacement of $q_p(T_c)$ to lower temperatures T_c and an increase in the maximum value of $q_p(T_c)$. The position and amplitude of the power flux density for the temperature-dependent work function is defined by the choice of the transition temperature T_{th}. For $T_{th} = 3000\,\mathrm{K}$ it is mainly determined by the trailing edge of $q_p(T_c)$ for $\phi = \phi_2$. It is represented by a high, narrow maximum. By the choosing of $T_{th} = 3000\,\mathrm{K}$ the power flux density of the temperature-dependent work function is placed between the courses of $q_p(T_c)$ for ϕ_1 and ϕ_2.

6. Simulation of the hot core mode

The existence range of the hot core mode is strongly dependent on the transition temperature T_{th} and the width of the transition zone τ between the work function $\phi_1 = 4.55\,\mathrm{eV}$ and $\phi_2 = 3\,\mathrm{eV}$. As an example the CVC of a hot core mode for $T_{th} = 3000\,\mathrm{K}$ and $\tau = 20\,\mathrm{K}$ is shown in figure 7. The electrode dimensions are $r_E = 300\,\mu\mathrm{m}$, $l_E = 10\,\mathrm{mm}$, and $r_{edge} = 37.5\,\mu\mathrm{m}$. It consists of two branches, which are linked in the reversal point of the CVC at the maximum current $i_{arc,max} = 14.3\,\mathrm{A}$. At currents above $i_{arc,max}$ a hot core mode cannot be verified for the special choice of T_{th} and τ by simulation.

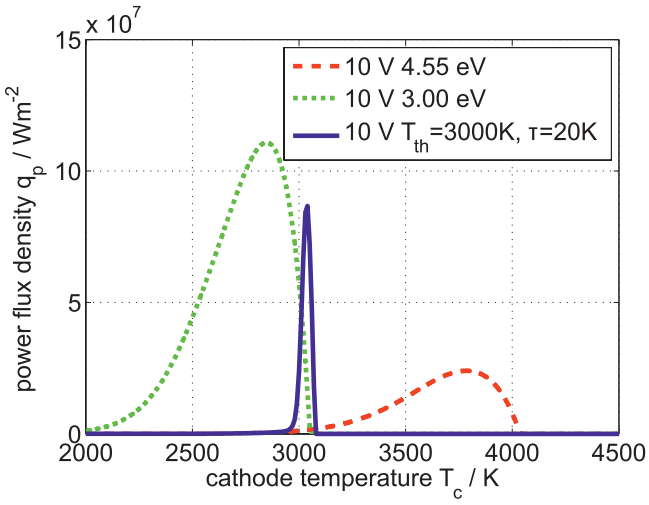

Figure 6. Examples for the power flux densities q_p in dependence on the local cathode temperature T_c for $U_c = 10$ V and different work functions ϕ. Red curve: $\phi_1 = 4.55$ eV; green curve: $\phi_2 = 3$ eV; blue curve: $\phi(T_c) = w_1(T_{th}, \tau)\phi_1 + w_2(T_{th}, \tau)\phi_2$ with $T_{th} = 3000$ K and $\tau = 20$ K.

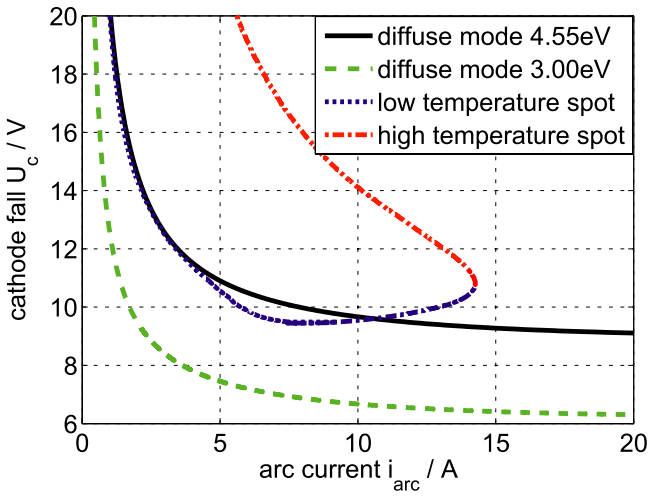

Figure 7. $U_c(i_{arc})$ of the hot core mode of cathodic arc attachment of an atmospheric pressure argon arc ($p = 0.1$ MPa) on a thoriated tungsten electrode with the dimensions $r_E = 300\,\mu$m, $l_E = 10$ mm and $r_{edge} = 37.5\,\mu$m. The work function applied to simulation is given by $\phi(T_c) = w_1(T_{th}, \tau)\phi_1 + w_2(T_{th}, \tau)\phi_2$; $\phi_1 = 4.55$ eV; $\phi_2 = 3$ eV; $T_{th} = 3000$ K, $\tau = 20$ K. In addition $U_c(i_{arc})$ of the diffuse mode of arc attachment for $\phi_1 = 4.55$ eV and $\phi_2 = 3$ eV are given.

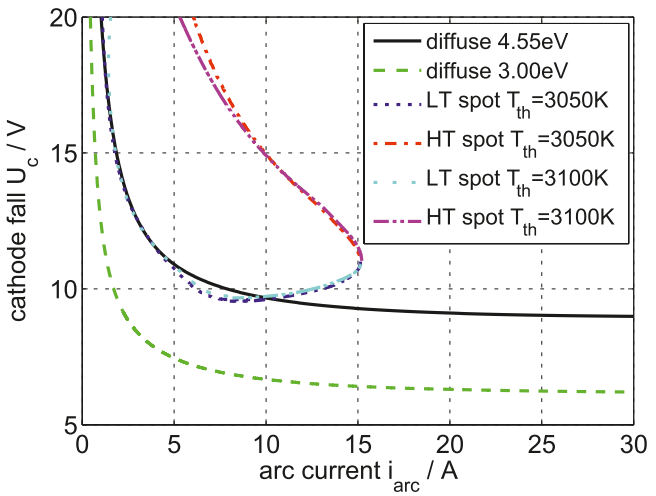

Figure 8. $U_c(i_{arc})$ of the hot core mode of cathodic arc attachment of an atmospheric pressure argon arc ($p = 0.1$ MPa) on a thoriated tungsten electrode with the dimensions $r_E = 300\,\mu$m, $l_E = 10$ mm, and $r_{edge} = 37.5\,\mu$m. The work function applied to simulation is given by $\phi(T_c) = w_1(T_{th}, \tau)\phi_1 + w_2(T_{th}, \tau)\phi_2$; $\phi_1 = 4.55$ eV; $\phi_2 = 3$ eV; $T_{th} = 3050$ K, $\tau = 20$ K and $T_{th} = 3100$ K, $\tau = 20$ K. Deviations of $U_c(i_{arc})$ for $T_{th} = 3100$ K from $U_c(i_{arc})$ for $T_{th} = 3050$ K are indicated by broken lines. Supplementary $U_c(i_{arc})$ of the diffuse mode of arc attachment for $\phi_1 = 4.55$ eV and $\phi_2 = 3$ eV are given.

This means that two solutions are found by simulation for a given arc current $i_{arc} < i_{arc,max}$. Similar CVCs were already previously obtained by the simulation of spot modes on pure tungsten electrodes [10, 11, 36]. Supplementary the CVCs of the diffuse mode for ϕ_1 and ϕ_2 are given which were already presented in [27], figure 9. The cathode falls of a diffuse mode at an electrode characterized by a work function $\phi_2 = 3$ eV are distinctly lower than those of the hot core mode for a given arc current. But for $\phi_1 = 4.55$ eV the cathode falls U_c of the diffuse mode are not very different to the cathode falls of the lower branch of the hot core mode. The cathode falls almost coincide for $i_{arc} < 3.5$ A and also the maximum values of the cathode temperature $T_{c,max}$ are quite similar. But the temperature distributions within the arc attachment zone of the diffuse mode and the hot core mode are substantially different.

The current maximum $i_{arc,max} = 14.3$ A for the special choice of parameters T_{th} and τ is lower than the arc current at which a hot core mode was observed experimentally. It becomes even lower for $T_{th} < 3000$ K and $\tau > 20$ K. But for $T_{th} = 3050$ K and $\tau = 20$ K the reversal point of the corresponding CVC given in figure 8 is displaced to $i_{arc,max} \geqslant 15$ A. Although the shape of the CVC is not very different to that for $T_{th} < 3000$ K, a better agreement is achieved with the experimental finding. A further increase in the transition temperature to $T_{th} = 3100$ K does not change the CVC and with it $i_{arc,max}$ distinctly. Only for $U_c > 15$ V the upper branch is bended to lower currents and the lower branch to higher currents indicating the formation of a closed loop by the CVC. The turning point of the CVC can be displaced to higher values of $i_{arc,max}$ by a reduction in the width of the transition zone to values of $\tau < 20$ K. But then it becomes difficult to get convergent solutions by the simulation procedure. For $T_{th} > 3100$ K again a reduction in $i_{arc,max}$ is found.

In figure 9 the power flux densities in dependence on the local cathode temperature $q_p(T_c)$ are given for $T_{th} = 3050$ K, $\tau = 20$ K and cathode falls U_c being varied in steps of 1 V from 8 to 20 V. The maximum values of the cathode temperature $T_{c,max}$ of the hot core mode represented by the CVC in figure 8 are marked on the curves $q_p(T_c, U_c = \text{const})$ in figure 9. The courses of $q_p(T_{c,max})$ in figure 9 reflects the two branches in figure 8. Considering the lower branch for $i_{arc} < 3.5\,\text{A} \cap U_c > 12$ V a maximum temperature $T_{c,max} \approx 3100$ K is found. It corresponds for $i_{arc} < 3.5$ A to T_{tip} of a diffuse mode on a pure tungsten electrode ($\phi = 4.55$ eV) with the same dimensions as is shown in [27], figure 4. But the maximum power flux

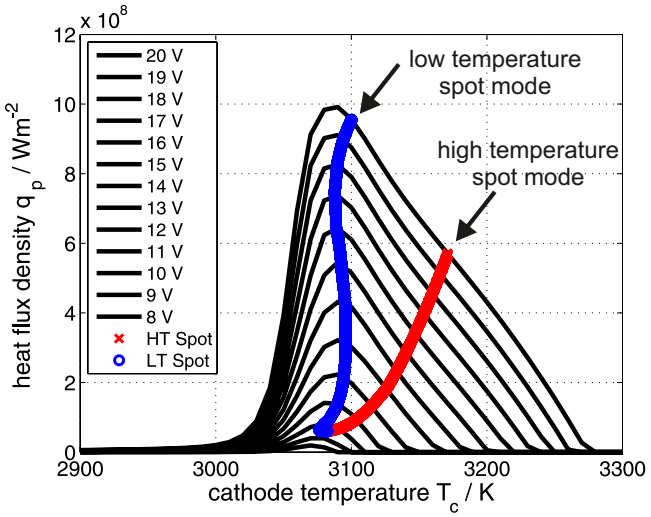

Figure 9. $q_\mathrm{p}(T_\mathrm{c}, U_\mathrm{c} = \mathrm{const})$ for a hot core mode of cathodic arc attachment of an atmospheric pressure argon arc ($p = 0.1$ MPa), simulated with a temperature-dependent work function characterized by $T_\mathrm{th} = 3050$ K and $\tau = 20$ K. The parameter U_c is varied from 8 to 20 V. In addition, for the maximum values of the cathode temperature $T_{\mathrm{c,max}}(U_\mathrm{c})$, the corresponding heat flux densities $q_\mathrm{p}(T_{\mathrm{c,max}})$ are plotted. Electrode dimensions $r_\mathrm{E} = 300\,\mu$m, $l_\mathrm{E} = 10$ mm and $r_\mathrm{edge} = 37.5\,\mu$m.

density $q_\mathrm{p}(T_{\mathrm{c,max}})$ of the hot core mode is of the order of 10^8–10^9 Wm^{-2} according to figure 9 whereas the power flux density $q_\mathrm{p}(T_\mathrm{tip})$ of the diffuse mode is of the order of 10^6–10^7 Wm^{-2} [10, 36]. Experimentally only a diffuse mode is observed for $i_\mathrm{arc} < 5$ A. The diagrams of q_p in dependence on T_c and the courses $q_\mathrm{p}(T_{\mathrm{c,max}})$ therein for $T_\mathrm{th} = 3000$ K, $\tau = 20$ K and $T_\mathrm{th} = 3100$ K, $\tau = 20$ K differ mainly by a shift of $\Delta T_\mathrm{c} \approx \pm 50$ K from the diagram for $T_\mathrm{th} = 3050$ K, $\tau = 20$ K, given in figure 9. Therefore, their presentation is omitted. For both solutions $q_\mathrm{p}(T_{\mathrm{c,max}})$ is positioned on the right-hand side of the maximum of the corresponding $q_\mathrm{p}(T_\mathrm{c})$-curve indicating that both solutions are stable according to the criterion given in [39, 40].

In addition courses of $j(r)$, $T_\mathrm{e}(r)$, $T_\mathrm{h}(r)$ and $T_\mathrm{c}(r)$ on the end face of the cathode are shown in figure 10 for $T_\mathrm{th} = 3050$ K, $\tau = 20$ K. Results are only given for the flat part of the end face extending from $r = 0$ to $r = 262.5\,\mu$m. An arc current $i_\mathrm{arc} = 12.5$ A was chosen to represent typical results since for this current and the same electrode detailed spectroscopic measurements were already published [4]. Distinctly different dependences on r are obtained for the solutions related to the upper and lower branches of the CVC. They are compared in figure 10.

The courses of $j(r)$, given in figure 10(a), show for both solutions a constriction of the current flow onto the centre of the end face. It is much more pronounced for the 'upper branch' solution than for the 'lower branch' solution. The distribution obtained for the upper branch is characterized by a width $2r_\mathrm{a,u} = 190\,\mu$m FWHM and that obtained for the lower branch by a width $2r_\mathrm{a,l} = 340\,\mu$m FWHM. The width of the corresponding course of $j(r)$ at a distance of $z = 50\,\mu$m given in figure 3(b) amounts to $2r_\mathrm{a,exp} = 590\,\mu$m FWHM and the maximum value of the current density in figure 3(b) $j(r = 0) = 7 \times 10^7$ Am^{-2}, which is of the same order of magnitude as $j(r = 0) = 14 \times 10^7$ Am^{-2} for the lower branch solution. Similar courses as for $j(r)$ are obtained for $T_\mathrm{e}(r)$ in figure 10(b). The maximum electron temperature amounts to $T_{\mathrm{e,max}}(r) = 35\,500$ K for the 'upper branch' solution and $T_{\mathrm{e,max}}(r) = 22\,800$ K for the 'lower branch' solution. In figure 2(b) an electron temperature $T_\mathrm{e}(r = 0, z = 0) \approx 22\,000$ K was found by extrapolation for $i_\mathrm{arc} = 12.5$ A.

In figure 10(c) the courses of the heavy particle temperature $T_\mathrm{h}(r)$ for the 'lower branch' and 'upper branch' solution are given. The $T_\mathrm{h,l}(r)$-profile obtained for the 'lower branch' solution is nearly box-shaped with $T_\mathrm{h,l}(r = 0) \approx 6600$ K and a steep decrease at $2r_\mathrm{a,l} = 340\,\mu$m to $T_\mathrm{h,edge}(r = r_E - r_\mathrm{edge}) \approx 3900$ K at the edge of the end face. It is in accordance with the other radial profiles of the 'lower branch' solution. The extrapolated heavy particle temperature in figure 2(b) $T_\mathrm{h}(r = 0, z = 0) \approx 11\,000$ K for $i_\mathrm{arc} = 12.5$ A is distinctly higher than $T_\mathrm{h,l}(r = 0)$.

The $T_\mathrm{h,u}(r)$-profile for the 'upper branch' solution looks at least in parts quite strange. The heavy particle temperature $T_\mathrm{h,u}(r = 0) = 3130$ K does not differ from the electrode temperature $T_\mathrm{c,u}(r = 0)$, given in figure 10(d). This means, according to equation (9), that the ohmic heating of the ions within the pre-sheath is balanced by the power, which is removed by the ion current from the pre-sheath. The reason for the high power transport by the ion current is the high electron temperature within the cathodic boundary layer of the 'upper branch' solution. The temperature peak at $r \approx 100\,\mu$m is an artefact which results from a steeper decrease in the electron temperature compared with the ohmic heating of the ions. The heavy particle temperature at the edge of the end face $T_\mathrm{h,edge}$ exceeds for the 'upper branch' solution the corresponding cathode temperature $T_\mathrm{c,edge}$ only marginally indicating that the power input into the cathodic boundary layer is low at the edge.

The result for $T_\mathrm{h,u}(r)$ related to the 'upper branch' solution shows the limitation of the cathodic boundary layer model. Presumably the neglect of two effects is mainly responsible for the unrealistic result. Even at high electron temperatures double ionization is not taken into account. Furthermore, the heating of the heavy particles by electron collisions is neglected, but may be important at high charged particle densities.

The courses of the electrode temperature T_c for the 'upper branch' and 'lower branch' solution, given in figure 10(d), have a similar shape as those of $j(r)$ and $T_\mathrm{e}(r)$. Only the radial gradients are less pronounced. The T_c-profile of the 'upper branch' solution reflects a distinct concentration of the power input $q_\mathrm{p}(r)$ onto the middle of the end face, as is indicated by the increase in the cathode temperature from $T_\mathrm{c,edge} \approx 2930$ K at the edge to $T_\mathrm{c}(r = 0) \approx 3130$ K in the centre of the end face. The T_c-profile of the 'lower branch' solution shows a moderate concentration of the power input $q_\mathrm{p}(r)$ as is indicated by a temperature increase from $T_\mathrm{c,edge}(r = 0) \approx 3035$ K at the edge to $T_\mathrm{c}(r = 0) \approx 3095$ K in the centre of the end face. It has to be pointed out that the edge temperature $T_\mathrm{c,edge}$ is more than 100 K higher in the case of the 'lower branch' solution than for the 'upper branch' solution. The temperature $T_\mathrm{c}(r = 0)$ of both hot core modes is, according to [27], figure 4, for $i_\mathrm{arc} = 12.5$ A

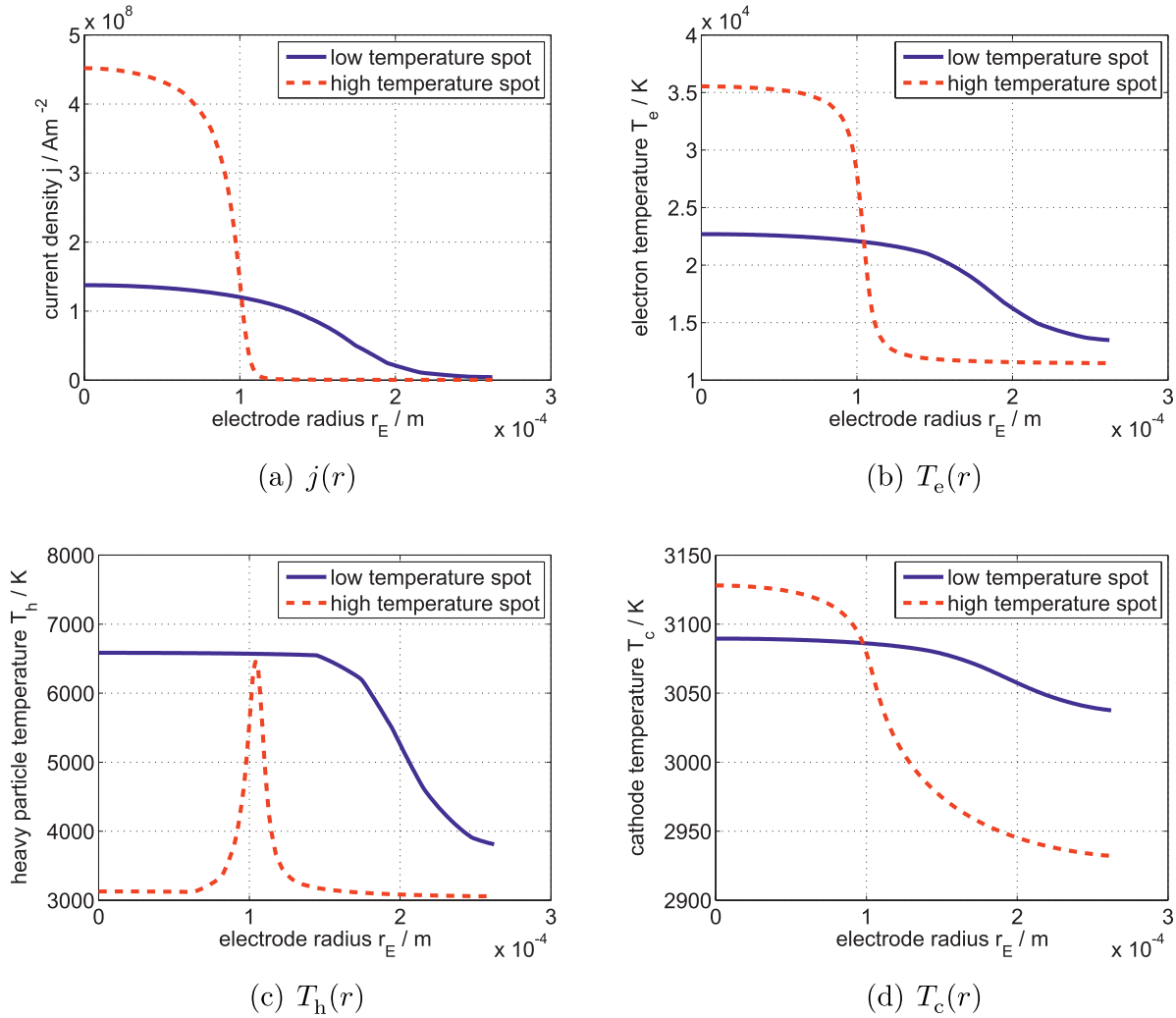

Figure 10. Radial distributions of characteristic quantities in front of or at the end face of the electrode within the hot core mode of cathodic arc attachment. (*a*) Upper left diagram: current densities $j(r)$. (*b*) Upper right diagram: electron temperatures $T_e(r)$. (*c*) Lower left diagram: heavy particle temperatures $T_h(r)$. (*d*) Lower right diagram: electrode temperatures $T_c(r)$. In each diagram a curve for the upper branch solution and the lower branch solution is given, obtained by simulation of an atmospheric pressure 12.5 A argon arc on a thoriated tungsten electrode. Electrode dimensions: $r_E = 300\,\mu$m, $l_E = 10$ mm and $r_{edge} = 37.5\,\mu$m. Work function: $\phi(T_c) = w_1(T_{th}, \tau)\phi_1 + w_2(T_{th}, \tau)\phi_2$; $\phi_1 = 4.55$ eV; $\phi_2 = 3$ eV; $T_{th} = 3050$ K, $\tau = 20$ K.

higher than the tip temperature $T_{tip} \approx 2650$ K produced by the diffuse mode on the same thoriated tungsten cathode, but distinctly lower than $T_{tip} \approx 3650$ K of the diffuse mode on a pure tungsten cathode with the same dimensions. However, as was already shown above, the difference between $T_c(r = 0)$ of the 'lower branch' solution and the tip temperature T_{tip} of a diffuse arc attachment on a pure tungsten cathode with the same dimensions shrinks with decreasing arc current.

7. Validation of the emitter spot model by comparison with measurements

For comparison with measurements the same radial distributions as for $i_{arc} = 12.5$ A given in figure 10 are calculated for $i_{arc} = 7.5, 10.0$ and 15.0 A. However, the comparison between measurements and simulation is rather difficult as the discussion of the results in figure 10 has already shown. The obstacle is that the simulation delivers plasma parameters within a layer of some micrometres thickness immediately in front of the cathode surface, but temperature and density measurements were only possible at a distance of 50 μm from the electrode surface. Therefore, a detailed comparison of radial profiles is not useful. But the variation of the plasma parameters in dependence on the arc current represents meaningful information which can be compared.

In figure 11(*a*) the FWHM of the current distribution $j(r)$, denoted by $d_{j,s}$, is given in dependence on the arc current i_{arc} for the lower and upper $U_c(i_{arc})$-branch solution. The $d_{j,s}$-values of both branches converge for $i_{arc} = 15$ A, but are distinctly higher for the lower branch solution for $i_{arc} < 15$ A. In addition for $i_{arc} = 7.5$, 10.0, 12.5 and 15.0 A the FWHM of the current distributions in figure 3(*b*), denoted by $d_{j,exp}$, and the FWHM of the intensity distributions immediately in front of the cathode d_{int}, taken from figure 1 are inserted. The values of $d_{j,exp}(i_{arc})$ and $d_{int}(i_{arc})$ approximately coincide. However, they are much larger than $d_{j,s}$, obtained for the upper $U_c(i_{arc})$-branch solution and also by a factor two larger than $d_{j,s}$ of

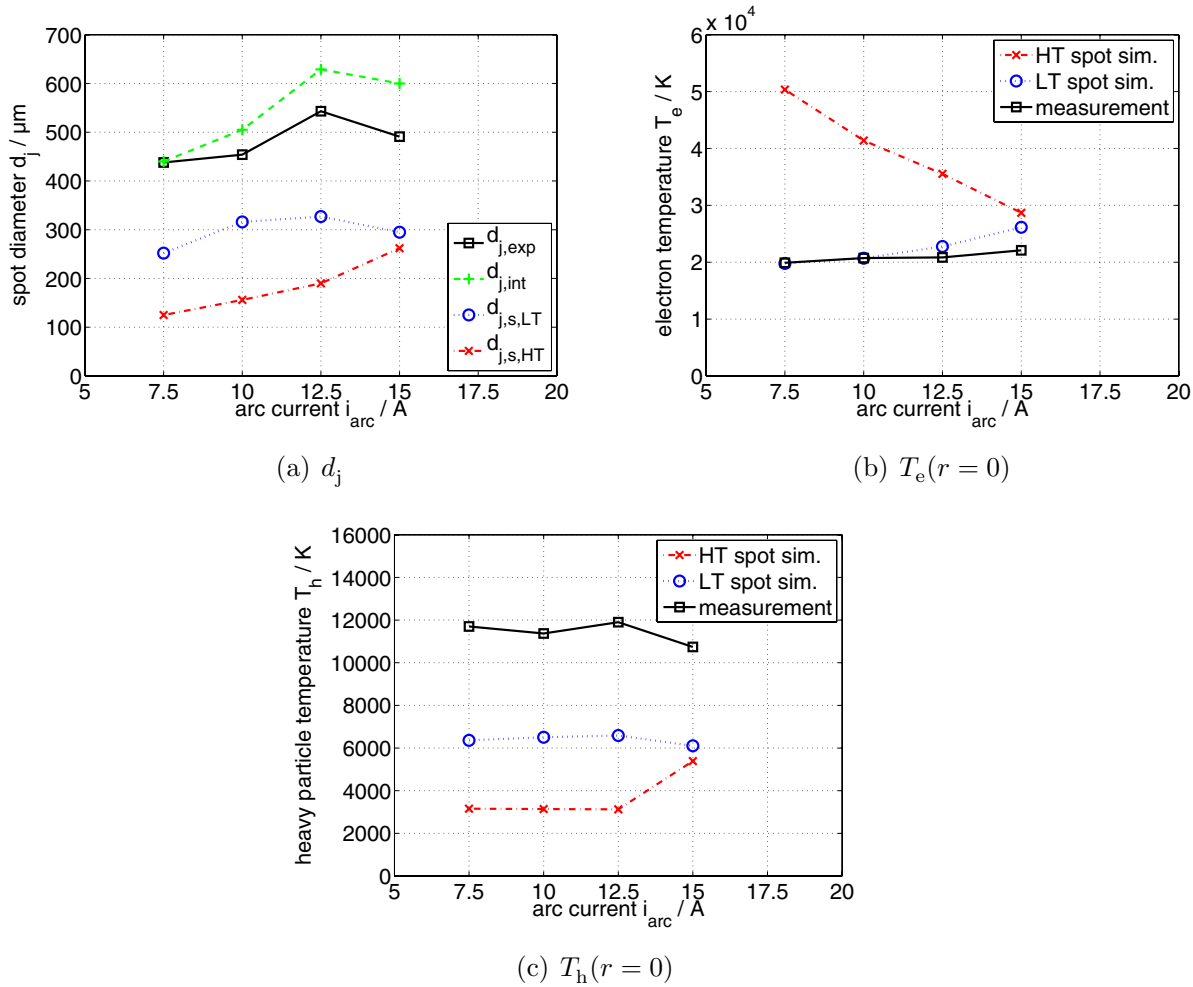

Figure 11. Characteristic quantities of the lower and upper $U_c(i_{arc})$-branch in dependence on i_{arc} from simulation and comparison with experimental findings for $i_{arc} = 7.5$, 10.0, 12.5 and 15.0 A. (*a*) FWHM of $j(r)$ determined by simulation, $d_{j,s,LT}$ and $d_{j,s,HT}$, FWHM of $j(r)$ given in figure 3(*b*), $d_{j,exp}$, and of the intensity distribution in front of the cathode, d_{int}, taken from figure 1. (*b*) Maximum values of the electron temperature $T_e(r = 0)$ within the cathodic boundary layer and $T_e(r = 0, z = 0)$ taken from figure 2(*b*). (*c*) Heavy particle temperature $T_h(r = 0)$ within the cathodic boundary layer and $T_h(r = 0, z = 50\,\mu m)$ taken from figure 2(*b*). Electrode dimensions: $r_E = 300\,\mu m$, $l_E = 10$ mm and $r_{edge} = 37.5\,\mu m$. Work function: $\phi(T_c) = w_1(T_{th}, \tau)\phi_1 + w_2(T_{th}, \tau)\phi_2$; $\phi_1 = 4.55$ eV; $\phi_2 = 3$ eV; $T_{th} = 3050$ K, $\tau = 20$ K.

the lower branch solution. The difference between $d_{j,s}$ of the lower branch solution and $d_{j,exp}$ or $d_{j,int}$ can be attributed to the different distances of approximately 50 μm from the electrode surface.

Figure 11(*b*) shows the courses of the maximum values of the electron temperature $T_e(r = 0)$ within the cathodic boundary layer in dependence on the arc current for the lower and upper $U_c(i_{arc})$-branch. A comparison with $T_e(r = 0, z = 0)$ determined in figure 2(*b*) by extrapolation for $i_{arc} = 7.5$, 10.0, 12.5 and 15.0 A shows a remarkable good agreement with the numerical results for the lower $U_c(i_{arc})$-branch. The values of $T_e(r = 0)$ obtained for the upper $U_c(i_{arc})$-branch solution differ from the measured values so much that it is quite impossible to explain them by an incorrect extrapolation in figure 2(*b*) in front of the electrode surface. The good agreement between the extrapolated and simulated electron temperature of the lower branch solution $T_e(r = 0, z = 0)$ may be attributed to the intense electron enthalpy flow from the cathodic boundary layer into the bulk plasma, by which the region of high electron temperature is broadened in front of the cathode. This is also indicated by the blue region in front of the cathode in figure 1.

Figure 11(*c*) presents the heavy particle temperature $T_h(r = 0)$ in front of the centre of the electrode end face for the lower as well as for the upper $U_c(i_{arc})$-branch solution in dependence on the arc current. Additionally, measuring values for $T_h(r = 0, z = 0)$ determined in figure 2(*b*) at $i_{arc} = 7.5$, 10.0, 12.5 and 15.0 A by extrapolation are shown. The measured temperatures $T_h(r = 0, z = 0)$ range over 10 000–12 000 K. The heavy particle temperatures of the upper $U_c(i_{arc})$-branch solution are scarcely higher than the cathode tip temperature T_c, and the temperatures $T_h(r = 0)$ of the lower $U_c(i_{arc})$-branch solution are between both. The differences between the experimentally determined temperatures $T_h(r = 0, z = 0)$ and the heavy particle temperatures delivered by the lower branch solution may be the result of an insufficient extrapolation in figure 2(*b*) but also of a deficit of the boundary layer model. But the lower branch solution represents a

better approximation of the experimental results than the upper branch solution.

The comparison between results of simulation and experimental results in figure 11 indicates a quite good approximation of the hot core mode by the lower branch solution of the emitter spot model. An outstanding result is the good agreement between the measured and simulated electron temperature within the boundary layer of the emitter spot, given in figure 11(*b*). But further experimental investigations are needed to ensure that the lower branch solution is the only one which can be realized experimentally.

8. Concluding remarks

It is shown that the measuring results agree well with the corresponding results of simulation by an emitter spot model, if they are compared with the lower $U_c(i_{arc})$-branch solution of the model. It confirms that the so-called 'hot core' mode of arc attachment on a thoriated tungsten cathode can be interpreted as an emitter spot.

The emitter spot does not disturb the rotational symmetry of the lamp discharge. Therefore, it interferes much less with a stable operation of HID lamps than the edge spot which may initiate a helical instability of the lamp arc [41–43] especially if the filling gas pressure within the lamp is high and the electrode distance large. But in the case of an ac operation the formation of an emitter spot within the cathodic phase and its disappearance within the anodic phase may excite acoustic oscillations within the lamp tube as is shown in [44].

It can be asserted generally that the hot core mode is induced by a thorium ion current in front of the cathode. It represents a quite good investigated example of an emitter spot.

Acknowledgments

The paper is based on a corporate research project on HID lamp electrodes, which was performed with financial support from the Federal Ministry of Education and Research in Germany (BMBF, project ref. no 13N6859, 13N7106/0, 13N7763). The authors bear in remembrance the dedicative coordination of the project by the late Professor Dr W Bötticher.

The authors would also like to thank Professor Dr Manfred Kock and Dr Jens Reiche for valuable discussions. Financial support from the Research School of the Ruhr University Bochum is also gratefully acknowledged by the authors.

References

[1] Reiche *et al* 2001 *J. Phys. D: Appl. Phys.* **34** 3177–84
[2] Könnemann *et al* 2004 *J. Phys. D: Appl. Phys.* **37** 171–9
[3] Kühn G and Kock M *et al* 2006 *J. Phys. D: Appl. Phys.* **39** 2401–14
[4] Kühn G and Kock M *et al* 2007 *Phys. Rev.* E **75** 016406
[5] Lichtenberg S *et al* 2002 *J. Phys. D: Appl. Phys.* **35** 1648–56
[6] Hartmann T *et al* 2002 *J. Phys. D: Appl. Phys.* **35** 1657–67
[7] Redwitz M *et al* 2005 *J. Phys. D: Appl. Phys.* **38** 3143–54
[8] Langenscheidt O *et al* 2007 *J. Phys. D: Appl. Phys.* **40** 415–31
[9] Reinelt J *et al* 2008 *J. Phys. D: Appl. Phys.* **41** 144002
[10] Dabringhausen L *et al* 2005 *J. Phys. D: Appl. Phys.* **38** 3128–42
[11] Benilov M S *et al* 2006 *J. Phys. D: Appl. Phys.* **39** 2124–34
[12] Lichtenberg S *et al* 2005 *J. Phys. D: Appl. Phys.* **38** 3112–27
[13] Benilov M S and Cunha M D 2002 *J. Phys. D: Appl. Phys.* **35** 1736–50
[14] Luijks G M J F *et al* 2005 *J. Phys. D: Appl. Phys.* **38** 3163–9
[15] Langenscheidt O *et al* 2008 *J. Phys. D: Appl. Phys.* **41** 144005
[16] Westermeier M *et al* 2008 *IEEE Trans. Plasma Sci.* **16** 1176–7
[17] Ruhrmann C *et al* 2014 *Contrib. Plasma Phys.* **54** 215–24
[18] Ruhrmann C 2014 Investigation of the emitter effect induced by rare earth elements in HID lamps *PhD Thesis* Ruhr University Bochum
[19] Ruhrmann C *et al* 2012 Influence of a cold spot heating on the emitter effect of an HID lamp: spectroscopic and pyrometric measurements *Proc. 13th Int. Symp. on the Science and Technology of Light Sources (Troy, NY)* ed R Devonshire and G Zissis CP036 167-8
[20] Reinelt J *et al* 2011 *J. Phys. D: Appl. Phys.* **44** 224006
[21] Westermeier M *et al* 2013 *J. Phys. D: Appl. Phys.* **46** 185201
[22] Westermeier M *et al* 2013 *J. Phys. D: Appl. Phys.* **46** 185202
[23] Ruhrmann C *et al* 2011 *J. Phys. D: Appl. Phys.* **44** 355202
[24] Ruhrmann C *et al* 2013 *J. Phys. D: Appl. Phys.* **46** 185202
[25] Hoebing T *et al* 2012 Investigations of the emitter-effect of Holmium in dimmed HID-lamps *Proc. 13th Int. Symp. on the Science and Technology of Light Sources (Troy, NY)* ed R Devonshire and G Zissis CP038 171-2
[26] Hartmann T *et al* 2010 *J. Phys. D: Appl. Phys.* **43** 025201
[27] Bergner A *et al* 2011 *J. Phys. D: Appl. Phys.* **44** 505203
[28] Dabringhausen L *et al* 2002 *J. Phys. D: Appl. Phys.* **35** 1621–30
[29] Redwitz M *et al* 2006 *J. Phys. D: Appl. Phys.* **39** 2160–79
[30] Mentel J and Heberlein J 2010 *J. Phys. D: Appl. Phys.* **43** 023002
[31] Kühn G 2005 Aktive und passive Plasmaspektroskopie im Kathodenbereich eines freibrennenden Lichtbogens, *PhD Thesis* University of Hannover
[32] Mitchener M and Kruger C H 1973 *Partially Ionized Gases* (New York: Wiley) p 51
[33] Benilov M S *et al* 2008 *J. Phys. D: Appl. Phys.* **41** 144001
[34] Benilov M S *et al* 2005 *Plasma Sources Sci. Technol.* **14** 517–24
[35] Benilov M S *et al* 2005 *J. Phys. D: Appl. Phys.* **38** 3155–62
[36] Scharf F H *et al* 2007 *Proc. 28th Int. Conf. on Phenomena in Ionized Gases (ICPIG) XXVIII (Prague, Czech republic, July 2007)* ed J Schmidt *et al* (Prague: Institute of Plasma Physics ASCR) pp 1252–5
[37] White G K and Minges M L 1997 *Int. J. Thermophys.* **18** 1269–327
[38] Yih S W H and Wang C T 1979 *Tungsten: Sources, Metallurgy, Properties and Applications* (New York: Plenum)
[39] Benilov M S 2007 *J. Phys. D: Appl. Phys.* **40** 1376–93
[40] Benilov M S and Faria M J 2007 *J. Phys. D: Appl. Phys.* **40** 5083–97
[41] Stoffels W W *et al* 2006 *Meas. Sci. Technol.* **17** N67–70
[42] Huelsmann H G and Mentel J 1987 *Phys. Fluids* **30** 2274–8
[43] Ernst K A *et al* 1973 *Z. Physik* 251–65
[44] Kettlitz M et al 2011 *J. Phys. D: Appl. Phys.* **44** 45205